Dalton Transactions

Stimuli-Responsive Metal-Organic Supercontainers as Synthetic Proton Receptors

Journal:	*Dalton Transactions*
Manuscript ID	DT-ART-05-2018-001900.R1
Article Type:	Paper
Date Submitted by the Author:	05-Jul-2018
Complete List of Authors:	Sun, Cheng-Zhe; Fujian Institute of Research on the Structure of Matter, Chinese Academy of Sciences; University of the Chinese Academy of Sciences Cheng, Li-Ji; Fujian Institute of Research on the Structure of Matter, Chinese Academy of Sciences Qiao, Yupu; University of South Dakota, Chemistry Zhang, Li-Yi; Fujian Institute of Research on the Structure of Matter, State Key Laboratory of Structural Chemistry Chen, Zhong-Ning; Fujian Institute of Research on the Structure of Matter, CAS, State Key Laboratory of Structural Chemistry Dai, Feng-Rong; Fujian Institute of Research on the Structure of Matter, Chinese Academy of Sciences, State Key Laboratory of Structural Chemistry Lin , Wei ; Northwestern University, Department of Chemistry Wang, Zhenqiang; University of South Dakota, Chemistry

Journal Name

ARTICLE

Stimuli-Responsive Metal-Organic Supercontainers as Synthetic Proton Receptors

Received 00th January 20xx,
Accepted 00th January 20xx

DOI: 10.1039/x0xx00000x

www.rsc.org/

Cheng-Zhe Sun,[a,d,†] Li-Ji Cheng,[a,†] Yupu Qiao,[b,†] Li-Yi Zhang,[a] Zhong-Ning Chen,*[a] Feng-Rong Dai,*[a] Wei Lin,*[c] and Zhenqiang Wang*[b]

We demonstrate a proof-of-concept design of a new platform for proton recognition and modulation. The new proton receptors are derived from a unique class of synthetic supercontainers that exhibit exceptional proton binding capacity (over 50 equiv.) and intriguing proton-dependent fluorescent switching behavior. Experimental and computational studies suggest that the proton-responsive event involves a two-step mechanism pertaining to proton binding by both amino and pyrenyl moieties of the supercontainer constructs. The high proton binding capacity of the supercontainers can be further modulated via small-molecule "regulators" that compete for the proton-binding sites, opening exiting new opportunities for proton manipulation in both chemistry and biology.

Introduction

Monitoring and regulating the proton is of fundamental interest in both chemistry and biology. For example, the proton occupies a central place in organic chemistry,[1, 2] whereas the intra- and extracellular *p*H levels play a pivotal role in many physiological and psychological conditions such as tumor growth, tissue repair, and panic disorder.[3-6] While proton-sensing G-protein-coupled receptors have been extensively studied and widely understood to be essential for maintaining cellular *p*H homeostasis,[4, 7, 8] studies of synthetic proton receptors are surprisingly limited and largely restricted to those based on small organic molecules with low proton binding capacity.[9-16] Proton recognition in metal-organic containers is particularly rare,[17] presumably due to the low acid-stability of most such systems. We recently developed a unique class of synthetic receptors, termed metal-organic supercontainers (MOSCs), which exhibit tunable molecular/ionic recognition capability,[18-25] and we were intrigued by the prospect of utilizing MOSCs as a new tool to recognize and manipulate proton activity. MOSCs are constructed from the assembly of three components, i.e., divalent metal ions (e.g., Co^{2+}, Zn^{2+}, etc.), sulfonylcalix[4]arene-based container precursors,[26-28] and carboxylate linkers of various shapes. A salient feature of MOSCs is their multi-pore architecture, possessing both *endo* and *exo* nanocavities within a single host molecule.[29, 30]

We contemplated that such a tunable and hierarchical structure would make MOSCs ideally suited as a new class of proton receptors.[9-16] We anticipated that three key elements fulfilling the design criteria of a functional proton receptor, namely, *proton recognition site*, *binding reporter*, and *regulatory domain*, can be readily incorporated into the MOSC construct (Scheme 1). For example, a judicious choice of proton binding group could be a Lewis base (e.g., an amine) inserted into the carboxylate linker, while the recognition signal may be derived from a luminescent[31] or electrochemical[24] mechanism; the unique MOSC architecture imparts additional desirable characteristics that facilitate not only the recognition but also, at least in principle, the regulation of the H^+ ion, distinguishing them from other types of proton receptors. Specifically, the multi-cavity structure of MOSCs could conceivably lead to a higher proton binding capacity, whereas the unique MOSC topology would allow ordered organization of multiple copies of the binding groups, giving rise to synergistic modulation of the recognition events. Herein, we describe a proof-of-concept study of proton receptor design based on these considerations. We show that the fluorescent emission of two rationally constructed MOSCs is responsive to their surrounding H^+ levels and that the exceptionally high and tunable binding capacity of the MOSCs can be harnessed to obtain an entirely new class of synthetic proton receptors.

We designed a 1,3-benzenedicarboxylate (1,3-BDC) derivative **L1** (Scheme 1), which belongs to the angular-planar type dicarboxylate linkers known to generate barrel-shaped

[a] State Key Laboratory of Structural Chemistry, Fujian Institute of Research on the Structure of Matter, Chinese Academy of Sciences, Fuzhou, Fujian 350002, China. E-mail: czn@fjirsm.ac.cn; dfr@fjirsm.ac.cn
[b] Department of Chemistry & Center for Fluorinated Functional Materials, University of South Dakota, 414 East Clark Street, Churchill-Haines Laboratories, Room 115, Vermillion, South Dakota 57069-2390, United States. E-mail: Zhenqiang.Wang@usd.edu
[c] Department of Chemistry, Northwestern University, Evanston, IL, 60208, United States. E-mail: Wei.Lin@northwestern.edu
[d] University of Chinese Academy of Sciences, Beijing 100049, China
† These authors contributed equally to this work.
Electronic Supplementary Information (ESI) available: experimental details and additional figures (PDF), and Crystallographic data (CIF). See DOI: 10.1039/x0xx00000x

"type-III" MOSCs when reacting with *p-tert*-butylsulfonylcalix[4]arene (TBSC) and divalent metal ions.[20] **L1** is imbedded with three desired constituents: a secondary amine (–NH–) serving as the principal proton binding site, a pyrenyl unit serving as the fluorescent tag, and a dicarboxylate moiety subtending a 120° angle expected to form type-III MOSC structures. The pyrenyl units may provide additional proton binding capacity via the now widely recognized "cation-π" interaction.[32-36]

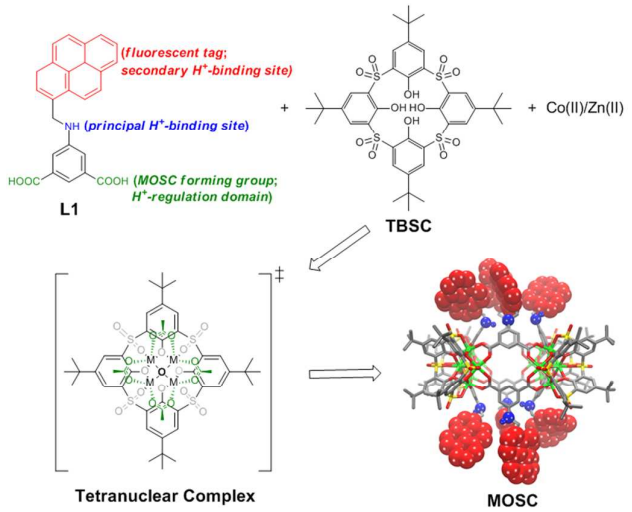

Scheme 1. Design of proton-responsive fluorescent MOSCs.

Experimental

General Methods.

Unless otherwise noted, starting materials and solvents were obtained from commercial suppliers and used without further purification. *p-tert*-Butylsulfonylcalix[4]arene (H_4TBSC)[27] was synthesized as described in the literature. UV-vis absorption spectra were measured on a Perkin-Elmer Lambda 35 UV-Vis spectrophotometer. The emission and excitation spectra were collected using an Edinburgh FLS-920 fluorescence spectrometer. Infrared spectra (IR) were recorded on a Magna 750 FT-IR spectrophotometer using KBr pellets as internal standard. Powder X-ray diffraction results were obtained from Rigaku Miniflex with Cu Kα radiation of λ = 1.5405 Å operated at 30 kV at the scan rate of 2 degree/min. Thermogravimetric analysis (TGA) was carried out on a Netzsch thermal analyzer (model-STA449C) at a heating rate of 5 °C/min under a constant nitrogen flow.

Synthesis

H_2**L1**, **(5-((pyren-1-ylmethyl)amino)isophthalic acid)**: 1-Pyrenecarboxaldehyde (2.30 g, 10 mmol) in methanol (50 mL) was added to a methanol solution (50 mL) of 5-aminoisophthalic acid (1.81 g,10 mmol) with stirring, upon which a brown solid formed immediately. The mixture was stirred at room temperature for 2 h. To the aforementioned mixture was added excess $NaBH_4$ (1.00 g, 26.00 mmol) in small portions over 5 minutes and the resulting mixture was stirred for additional 30 minutes. The mixture was then filtered off and the filtrate was dried by rotary evaporation. The residue was then dissolved in 100 mL water and the *p*H of the aqueous solution was adjusted to 5.0 using an HCl solution (1.0 mol L^{-1}). The off-white solid was collected, washed with water and diethyl ether, dried, and recrystallized from MeOH/H_2O (3:1). Yield: 2.40 g, 60%. ^{1}H NMR (400 MHz, DMSO-d_6): δ = 12.90 (s, 2H, -COOH), 8.47 (d, J = 9.32 Hz, 1H, Pyr-H), 8.29 (m, 4H, Pyr-H), 8.15 (s, 2H, Pyr-H), 8.08 (m, 2H, Pyr-H), 7.74 (s, 1H, Ar-H), 7.41 (s, 2H, Ar-H), 6.71 (t, J = 4.96 Hz, 1H, -NH-), 5.05 (d, J = 4.84 Hz, 2H, -CH_2-) ppm.

1-Co: $Co(NO_3)_2{\cdot}6H_2O$ (72.80 mg, 0.25 mmol), H_2**L1** (67.50 mg, 0.17 mmol) and H_4TBSC (42.50 mg, 0.05 mmol) were dissolved in a mixture solvent of DMF (5 mL) and methanol (4 mL) in a scintillation vial (20-mL capacity). The vial was placed in a sand bath, which was transferred to a programmable oven and heated at a rate of 0.5 °C/min from 30 to 100 °C. The temperature was held at 100 °C for 24 h before the oven was cooled at a rate of 0.2 °C/min to a final temperature of 30 °C. Pink crystals of **1-Co** were isolated by washing with DMF and acetone. Further solvent exchange experiments were performed by soaking the crystals in acetone for 3 days with the acetone solvent replenished four times. The crystals were then vacuum dried at 100 °C to give rise to 62 mg of activated material. Yield: 66%. Elemental analysis calcd (%) for $C_{465}H_{619}Co_{16}N_{33}O_{149}S_{16}$: C 53.13, H 5.94, N 4.40; Found: C 53.60, H 4.78, N 4.30. The empirical formula of **1-Co** is estimated to be $[Co_4(TBSC)(\mu_4\text{-}H_2O)]_4$(**L1**)$_8(DMF)_{25}(CH_3OH)_{30}(H_2O)_{10}$ based on TGA, elemental analysis, and SQUEEZE results.

1-Zn: $Zn(NO_3)_2{\cdot}6H_2O$ (74.50 mg, 0.25 mmol), H_2**L1** (67.50 mg, 0.17 mmol) and H_4TBSC (42.50 mg, 0.05 mmol) were dissolved in a mixture solvent of DMF (5 mL) and methanol (4 mL) in a scintillation vial (20-mL capacity). The vial was placed in a sand bath, which was transferred to a programmable oven and heated at a rate of 0.5 °C/min from 30 to 100 °C. The temperature was held at 100 °C for 24 h before the oven was cooled at a rate of 0.2 °C/min to a final temperature of 30 °C. Yellowish crystals of **1-Zn** were isolated by washing with DMF and acetone. Further solvent exchange experiments were performed by soaking the crystals in acetone for 3 days with the acetone solvent replenished four times. The crystals were then vacuum dried at 100 °C to give rise to 54 mg of activated material. Yield: 57%. Elemental analysis calcd (%) for $C_{440}H_{550}N_{32}O_{139}S_{16}Zn_{16}$: C 52.48, H 5.50, N 4.45; Found: C 51.82, H 5.28, N 4.52. The empirical formula of **1-Zn** is estimated to be $[Zn_4(TBSC)(\mu_4\text{-}H_2O)]_4$(**L1**)$_8(DMF)_{24}(CH_3OH)_8(H_2O)_{23}$ based on TGA, elemental analysis, and SQUEEZE results.

X-Ray Crystallography

X-ray single-crystal diffraction data were collected using graphite-monochromated Mo-Kα radiation (λ = 0.71073 Å) on a Rigaku Mercury CCD diffractometer. The CrystalClear software package was used for data reduction and empirical absorption correction. The structures were solved by the Direct methods (SHELX97)[37] in conjunction with standard difference Fourier techniques and subsequently refined by full-

matrix least-squares analyses on F^2. Hydrogen atoms were generated in their idealized positions and all non-hydrogen atoms were refined anisotropically. The electron count due to disorder solvent in the void space of the crystals was calculated using the program SQUEEZE in PLATON software package and refined further using the data generated.[38, 39] The contents of the removed solvents are not represented in the unit cell contents in the crystal data (Table S1). CCDC numbers 1821130-1821131 contain the supplementary crystallographic data for this paper. These data can be obtained free of charge from the Cambridge Crystallographic Data Centre via www.ccdc.cam.ac.uk/data_request/cif.

UV-vis and Fluorescent Spectroscopic Titration Experiments

Stock solutions of the MOSC (**1-Co** or **1-Zn**) were prepared in $CHCl_3$ at a concentration of ~5×10^{-6} M. 10.00 mL of the stock solution was then used to dissolve an accurately known mass of CF_3COOH, chosen to yield a solution at a concentration 50~100 times greater than that of the MOSC. 2.40 mL of the MOSC solution was placed in a 10.0 mm quartz cell, upon which 1 to 500 µl of the acid solution was added gradually. After each addition, the cell was stoppered and inverted, and the UV-Vis and fluorescent spectra were collected at room temperature after 5 minutes to ensure complete mixing and reaching equilibration.

^{19}F NMR Titration Experiments

A stock solution of CF_3COOH was prepared in $CDCl_3$ at a concentration of ~ 0.421 M. A small amount of the stock solution was then added in an incremental equivalent (2~70) to a solution of **1-Zn** in $CDCl_3$ (at ~ 4.59 mM). The resulting mixture was stirred for 2 hours at room temperature, filtered, and monitored by ^{19}F NMR on a Bruker 400 MHz NMR instrument.

Theoretical Calculations

All density functional theory calculations were performed using the Q-Chem software package.[40] A model compound, i.e., dimethyl ester of **L1** (designated as Me_2-**L1**), was selected as a surrogate for **1-Co**/**1-Zn**, as it is sufficiently representative of the principal chromophores in the MOSCs. The corresponding ground-state structures were optimized using the M06-L functional[41, 42] and the aug-cc-pVTZ basis set[43] was employed for all atoms in the system. During the optimization, the self-consistent field (SCF) convergence was set to 10^{-6} and the thresh cutoff was 10^{-11}.

Results and discussion

Two neutral MOSC molecules, designated as **1-Co** and **1-Zn**, were obtained as crystalline products from solvothermal reactions of H_2**L1**, TBSC, and $Co(NO_3)_2$ or $Zn(NO_3)_2$, respectively. Their structures were determined by single-crystal X-ray diffraction analysis (Table S1), which revealed an isostructural MOSC topology.[20] As in the original type-III MOSCs, **1-Co** and **1-Zn** feature a barrel-shaped *endo* cavity defined by the lower rims of four M_4(TBSC) moieties (known as "tetranuclear complexes"[44]; Scheme 1) and the aromatic walls of eight **L1** linkers; four cup-shaped *exo* cavities are each sustained by the upper rim of the TBSC unit (Figures S1-2). The *endo* cavity of **1-Co** and **1-Zn** exhibited two obstructed openings (Figure 1), each surrounded by four pyrenyl groups orderly assembled *via* edge-to-face π-π interactions (Figure S3), boding well for the potential proton recognition cooperativity.

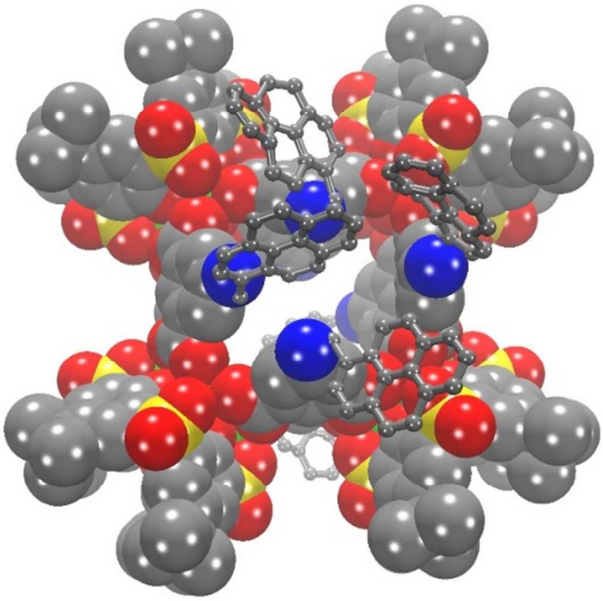

Figure 1. Structural depiction of **1-Co**/**1-Zn**. MOSC backbone is shown in space-filling mode, while pyrenyl groups are represented as balls and sticks (H atoms are deleted for clarity). Color scheme: C, gray; N, blue; O, red; S, yellow; Co/Zn: green.

The two MOSCs showed several characteristics highly desirable for proton recognition: they exhibit good solubility (up to 10^{-3} M in $CHCl_3$), robust thermal/chemical stability (Figures S4-7), and stimuli-responsive luminescent properties. The absorption spectrum of **1-Co** in $CHCl_3$ featured an intense absorption band centered at 348 nm, indicative of an intramolecular charge transfer process involving the Co_4(TBSC) tetranuclear units[19, 20] and possibly the pyrenyl groups as well. Three additional peaks, centered at 279, 290, and 397 nm, respectively, were attributed to the characteristic absorption of the pyrenyl groups.[45] The incorporation of the pyrenyl reporter into the MOSC construct led to only moderate luminescent emission of the MOSCs (Figure S8): for **1-Co**, an emission band centered at 417 nm and accompanied by two shoulders at 393 nm and 460 nm was observed upon excitation at 360 nm, which was attributed to the emissions of individual monomer (393 and 417 nm) and intramolecular excimer (460 nm) of the pyrenyl moiety;[46] the emission profile of **1-Zn** closely resembled that of **1-Co**, although with a less visible shoulder at shorter wavelengths.

The well-understood luminescent properties of **1-Co** and **1-Zn** allowed us to probe their *p*H-responsive behavior using spectroscopic titration techniques.[47-49] Trifluoroacetic acid

(TFA) was chosen as a proton source due to its strong acidity,[50] good solubility in $CHCl_3$ (i.e., a solvent in which the MOSCs are readily soluble), and convenience of monitoring MOSC protonation via ^{19}F NMR (*vide infra*). Upon adding incremental portions of a standard TFA solution to a **1-Co** or **1-Zn** solution and maintaining the TFA:MOSC molar ratio in the range of 1 ~ 250, we observed a gradual increase in peak intensity and small blue shift in peak position for the main absorption band centered at ~ 348 nm (Figures S8-10). This subtle UV-vis absorption response was attributed to the protonation of the principal proton binding sites (i.e., the –NH– groups). The proton-induced spectroscopic response of the MOSCs was further evidenced by their fluorescent profiles, which revealed an even more conspicuous response to the H^+ levels. Indeed, the fluorescent emission of **1-Zn** was enhanced by as much as 7 folds when treated with an excess amount of TFA (Figures 2 and S11). **1-Co** exhibited a similar proton-dependent fluorescent enhancement (Figure S12).

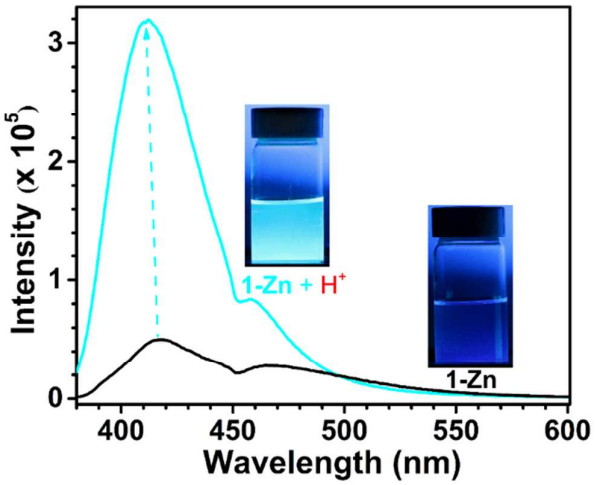

Figure 2. Fluorescent emission spectra of **1-Zn** before (black) and after (cyan) the addition of an excess amount of proton (from trifluoroacetic acid).

The *p*H-dependent spectroscopic response of **1-Co** and **1-Zn** was consistent with the proposed protonation of the –NH– groups, which disrupted the hyperconjugation system of the MOSC structure. This protonation event thus mitigated the otherwise emission-quenching process of electron transfer from the pyrenyl groups to the M_4(TBSC) tetranuclear units and led to the observed fluorescent enhancement.[51] This rationalization was supported by several lines of evidence. For example, the fluorescent switching of the MOSCs was fully reversible between acidic and basic conditions, as the emission of TFA-treated **1-Co**/**1-Zn** could be reduced to lower than the original intensity upon adding a base such as trimethylamine (Figures S13-14), and the "acid-enhancing, base-quenching" cycle could be repeated at least 10 times without noticeable fatigue (Figure 3 and Figure S15). An impressively high ratio (~10) of the emission maximum vs. minimum during the switching cycle was observed for **1-Zn**, whereas this ratio was somewhat smaller (~ 3.5) for **1-Co** (Figures S16-17). The relevance of the –NHR groups to the proton-binding capability of **1-Co**/**1-Zn** was further evidenced by their drastically enhanced acid-resistance, as indicated by their ability to retain structural integrity in the presence of large equivalents of TFA (Figure S9-10); in contrast, the original type-III MOSCs, containing no amino groups,[20] quickly decomposed upon addition of a small amount of TFA (Figure S18).

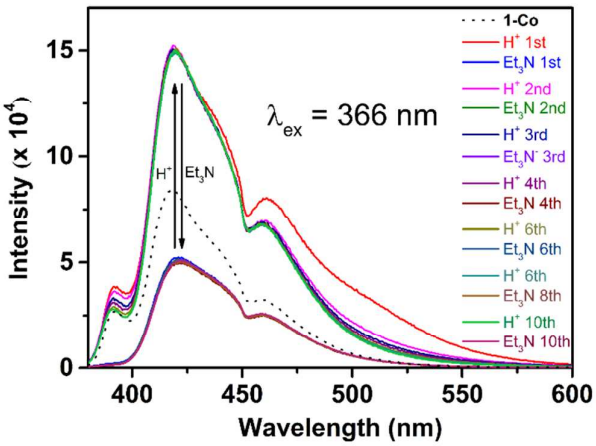

Figure 3. Switching "on" and "off" of **1-Zn** with CF_3COOH/Et_3N can be repeated multiple cycles.

The proposed mechanism was further corroborated by a computational analysis. A model compound, namely, dimethyl ester of **L1** (designated as Me_2-**L1**), was selected as a surrogate for **1-Co**/**1-Zn**, as it sufficiently represents the proton binding sites of the MOSCs. Density functional theory (DFT) at the M06-L/aug-cc-pVTZ level[52] was employed to probe the electronic structures of Me_2-**L1** before and after protonation (Figure S19). It was revealed that for neutral Me_2-**L1** molecule, its lowest-unoccupied molecular orbital (LUMO) is dispersed throughout the entire molecule, "homogenizing" the 1,3-BDC and pyrenyl units via the –NH– bridge (Figure 4, top). This result thus lent strong credence to the proposed charge-transfer mechanism, which accounts for the dampened luminescent emission of **1-Co**/**1-Zn**. In stark contrast, the LUMO of Me_2-**L1** upon protonation at the –NH– site was *exclusively* localized at the 1,3-BDC unit (Figure 4, bottom), indicating a disruption of the charge-transfer pathway and providing a convincing theoretical support for the observed proton-responsive fluorescent behavior of **1-Co**/**1-Zn**.

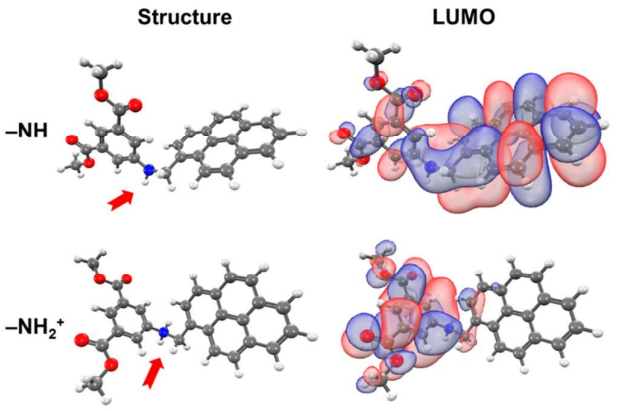

Figure 4. Lowest-unoccupied molecular orbital (LUMO) of model compound Me_2-**L1** before and after protonation at the –NH group.

The proton-binding capacity of **1-Co** and **1-Zn** can be quantified via a plot of fluorescent intensity vs. TFA equivalent (Figures S20-21). The fluorescent emission of both MOSCs correlated almost linearly with the H^+ concentrations at lower TFA loadings up to ~ 10 equiv., which is reasonably consistent with the eight principal proton-binding sites (i.e., –NH– groups) anticipated for each MOSC. Surprisingly, the emission saturated at a TFA equivalent drastically higher than one would have anticipated (i.e., over 50 equiv.). This exceptionally high proton-recognition capacity promoted us to contemplate an additional mechanism involving the pyrenyl groups serving as secondary proton-binding sites (e.g., via cation-π interaction[33-35]). The two-step proton-binding profile was indeed apparent from the aforementioned plots of fluorescent intensity vs. TFA equivalent (Figures S20-21). The two-step binding process was further validated by ^{19}F NMR titration experiments, in which a gradually increasing amount of TFA was added to a **1-Zn** solution and the up-field shift of the resulting CF_3COO^-/CF_3COOH species ($\Delta\delta_F$) was monitored as a function of the TFA/**1-Zn** molar ratio ($r_{TFA/\mathbf{1\text{-}Zn}}$). The $\Delta\delta_F$–$r_{TFA/\mathbf{1\text{-}Zn}}$ correlation suggested that the transition from the first to the second mechanism occurred at $r_{TFA/\mathbf{1\text{-}Zn}} \approx 8$~10, and that the ⍰⍰$_F$ value reached saturation at $r_{TFA/\mathbf{1\text{-}Zn}} \approx 30$~50 (Figure S22), both of which are in good agreement with the above fluorescent results.[53]

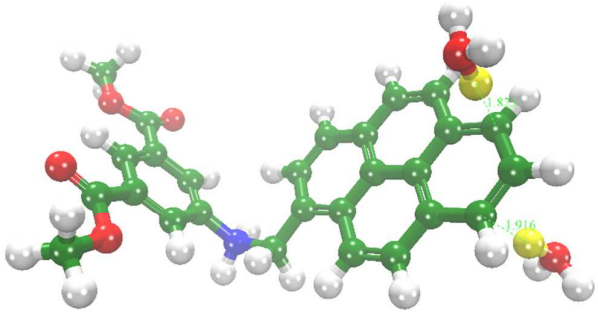

Figure 5. DFT calculation (at the M06-L/aug-cc-pVTZ level) of hydrogen bonding involving multiple H_3O^+ ions with peripheral carbon atoms from either side of the pyrenyl ring in *N*-protonated Me_2-**L1**.

To further shed light on the nature of the remarkable proton binding capacity of **1-Co** and **1-Zn**, we performed additional DFT calculations at the same M06-L/aug-cc-pVTZ level described earlier. When the hydronium ion (H_3O^+)[54] was placed above the pyrenyl ring, it was found to participate in an ionic hydrogen bond with a peripheral carbon atom (H···C = 1.76 Å; Figure S23), indicating a more extreme case of the conventional cation-π interaction. Since a number of the peripheral carbons (up to ~8; Figure 4) are available to form a similar ionic hydrogen bond with H_3O^+, and they can be accessed from either side of the pyrenyl ring to overcome steric hindrance, it is plausible to envision multiple protons simultaneously binding with each pyrenyl unit (Figure 5). Thus, the eight pyrenyl groups in each MOSC may accommodate up to ~64 additional protons, satisfactorily explaining the exceptional proton binding capacity of the MOSCs. The multi-proton binding capability of the pyrenyl unit was indeed confirmed by the DFT calculation (Figures 5 and S24-25). We note that the hydrated H_3O^+ and $H_7O_3^+$ ions were employed in our calculation, since the chloroform solvent was presumed to contain water. When the naked H^+ ion was used instead, it was found to *covalently* bind to a carbon atom (Figure S26); this observation was consistent with recent findings obtained using the more sophisticated resolution-of-identity second-order Møller-Plesset perturbation theory (RI-MP2).[36]

Finally, it is worth noting that the principal proton-binding sites of **1-Co**/**1-Zn** can be further addressed using selected neutral molecules serving as "modulators". When **1-Co** or **1-Zn** was treated with 1-pyrenecarboxaldehyde or 1-acetylpyrene, both of which contained a carbonyl group reactive toward the –NH– moiety, the fluorescent emission of the MOSCs was repressed precipitously (Figure 6 and Figures S27-29). It was clear that such fluorescent repression was not *directly* due to π-π stacking between the pyrenyl groups of the MOSC and the modulator, since titrating pyrene itself to **1-Co**/**1-Zn** did not cause any noticeable fluorescent quenching (Figure 7 and Figure S30). The aldehyde/ketone-induced fluorescent repression was thus attributed to the formation of an aminoalcohol species[55] through *covalent* binding between carbonyl group of the modulator and –NH– group of the MOSC (Figure 6). The lone-pair electrons on both nitrogen and oxygen atoms of the aminoalcohol amplified the hyperconjugation and enhanced the charge transfer, causing the fluorescence to diminish. The observation that larger aldehydes/ ketones led to more pronounced fluorescent quenching (i.e., it follows the trend: pyrenyl > anthracenyl > naphthyl > benzyl; Figures S31-36) indicates that the π-π interaction likely contributed to stabilizing the otherwise unstable aminoalcohol species, thus *indirectly* facilitating the quenching process. This observation suggests that it is potentially feasible to regulate the proton-binding behavior of the MOSCs using competitive or parallel modulations such as aldehydes and ketones (Figure S37), an exciting aspect we currently actively pursuing.

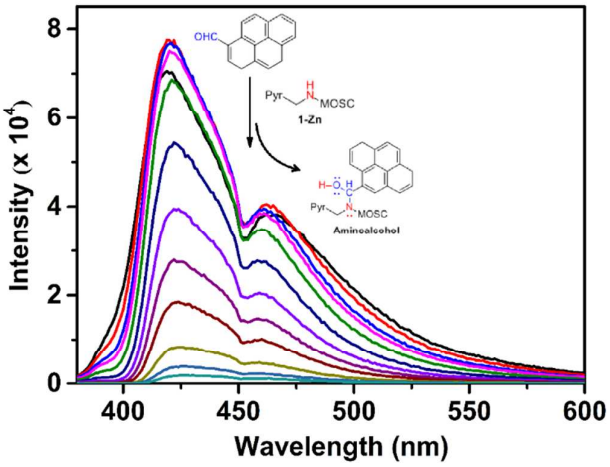

Figure 6. Fluorescent quenching of **1-Zn** when titrated with 1-pyrenecarboxaldehyde. The arrow indicates a gradual increase of 1-pyrenecarboxaldehyde equivalent. The inserted reaction scheme indicates a plausible pathway to regulate the H^+-binding capacity of the MOSCs.

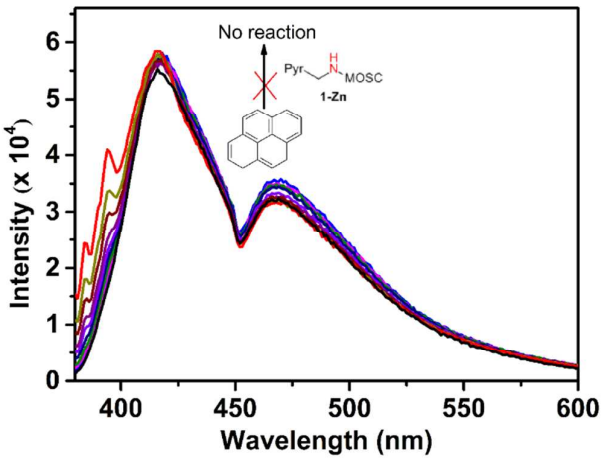

Figure 7. Emission spectra of **1-Zn** titrated with pyrene. The arrow indicates a gradual increase of pyrene equivalent.

Conclusions

We have demonstrated the design of a new proton recognition platform. The MOSC constructs chosen in this study are unique in several important aspects. Their robust acid stability allows a rare opportunity to explore new concepts of proton recognition using metal-organic supramolecular assemblies, which are otherwise often highly fragile under acidic conditions. The multiple proton binding pathways accessible and exceptional binding capacity of the MOSCs underline their great potential to serve not only as proton receptors, but also as potential proton modulators through regulated removal or release of the proton, an aspect we wish to investigate in biologically relevant settings. The feasibility of addressing the proton binding event in extra dimensions using basic or neutral organic molecules opens an even wider array of possibilities in which the MOSCs serving as proton receptors to regulate processes as diverse as Brønsted-acid catalysis and H_2S sensing can be envisioned.

Conflicts of interest

There are no conflicts to declare.

Acknowledgements

C.Z.S., L.J.C., Z.N.C. and D.F.R. thank the support of National Natural Science Foundation of China (Nos. 21673239, 21501179, 21473201 and 21390392), Natural Science Foundation of Fujian Province (No. 2017J06008), the 973 Project from MSTC (Grant 2014CB845603), the CAS/SAFEA International Partnership Program for Creative Research Teams, and the Strategic Priority Research Program of the Chinese Academy of Sciences (Grant XDB20000000); Z.W. and Y.Q. acknowledge financial support provided by National Science Foundation (CHE-1352279 and DMR-1709912) and South Dakota Governor's Office of Economic Development (through funding to the Center for Fluorinated Functional Materials).

Notes and references

1 R. Stewart, *The proton: applications to organic chemistry*, Academic Press, Orlando, 1985.

2 M. Rueping, D. Parmar and E. Sugiono, *Asymmetric Bronsted Acid Catalysis*, Wiley-VCH, 2016.

3 D. Neri and C. T. Supuran, *Nat. Rev. Drug Discov.*, 2011, **10**, 767-777.

4 K. T. Weiss, M. Fante, G. Kohl, J. Schreml, F. Haubner, M. Kreutz, S. Haverkampf, M. Berneburg and S. Schreml, *Exp. Dermatol.*, 2017, **26**, 127-132.

5 A. E. Ziemann, J. E. Allen, N. S. Dahdaleh, Drebot, I. I., M. W. Coryell, A. M. Wunsch, C. M. Lynch, F. M. Faraci, M. A. Howard, III, M. J. Welsh and J. A. Wemmie, *Cell*, 2009, **139**, 1012-1021.

6 J. R. Casey, S. Grinstein and J. Orlowski, *Nat. Rev. Mol. Cell Biol.*, 2010, **11**, 50-61.

7 M. G. Ludwig, M. Vanek, D. Guerini, J. A. Gasser, C. E. Jones, U. Junker, H. Hofstetter, R. M. Wolf and K. Seuwen, *Nature*, 2003, **425**, 93-98.

8 K. Seuwen and M.-G. Ludwig, in *Encyclopedia of Molecular Pharmacology*, eds. S. Offermanns and W. Rosenthal, Springer Berlin Heidelberg, Berlin, Heidelberg, 2008, DOI: 10.1007/978-3-540-38918-7_200, pp. 1035-1037.

9 J. Cheney and J. M. Lehn, *J. Chem. Soc., Chem. Commun.*, 1972, DOI: 10.1039/C39720000487, 487-489.

10 P. B. Smith, J. L. Dye, J. Cheney and J. M. Lehn, *J. Am. Chem. Soc.*, 1981, **103**, 6044-6048.

11 H. J. Bruegge, D. Carboo, K. Von Deuten, A. Knoechel, J. Kopf and W. Dreissig, *J. Am. Chem. Soc.*, 1986, **108**, 107-112.

12 A. P. de Silva, H. Q. N. Gunaratne and C. P. McCoy, *Chem. Comm.*, 1996, DOI: DOI 10.1039/cc9960002399, 2399-2400.

13 P. Bühlmann, E. Pretsch and E. Bakker, *Chem. Rev.*, 1998, **98**, 1593-1687.
14 L. Fabbrizzi, F. Gatti, P. Pallavicini and L. Parodi, *New J. Chem.*, 1998, **22**, 1403-1407.
15 A. J. Zucchero, J. N. Wilson and U. H. F. Bunz, *J. Am. Chem. Soc.*, 2006, **128**, 11872-11881.
16 J. Tolosa, A. J. Zucchero and U. H. F. Bunz, *J. Am. Chem. Soc.*, 2008, **130**, 6498-6506.
17 M. D. Pluth, R. G. Bergman and K. N. Raymond, *Science*, 2007, **316**, 85-88.
18 F.-R. Dai and Z. Wang, *J. Am. Chem. Soc.*, 2012, **134**, 8002-8005.
19 F.-R. Dai, U. Sambasivam, A. J. Hammerstrom and Z. Wang, *J. Am. Chem. Soc.*, 2014, **136**, 7480-7491.
20 F.-R. Dai, D. C. Becht and Z. Wang, *Chem. Commun.*, 2014, **50**, 5385-5387.
21 N. L. Netzer, F.-R. Dai, Z. Wang and C. Jiang, *Angew. Chem. Int. Ed.*, 2014, **53**, 10965-10969.
22 N. Bhuvaneswari, K. P. Annamalai, F.-R. Dai and Z.-N. Chen, *J. Mater. Chem. A*, 2017, **5**, 23559-23565.
23 Y. Qiao, L. Zhang, J. Li, W. Lin and Z. Wang, *Angew. Chem. Int. Ed.*, 2016, **55**, 12778-12782.
24 N. L. Netzer, I. Must, Y. Qiao, S. L. Zhang, Z. Wang and Z. Zhang, *Sci. Rep.*, 2017, **7**, 45786.
25 N. Bhuvaneswari, F. R. Dai and Z. N. Chen, *Chemistry – A European Journal*, 2018, **24**, 6580-6585.
26 H. Kumagai, M. Hasegawa, S. Miyanari, Y. Sugawa, Y. Sato, T. Hori, S. Ueda, H. Kamiyama and S. Miyano, *Tetrahedron Lett.*, 1997, **38**, 3971-3972.
27 N. Iki, H. Kumagai, N. Morohashi, K. Ejima, M. Hasegawa, S. Miyanari and S. Miyano, *Tetrahedron Lett.*, 1998, **39**, 7559-7562.
28 N. Morohashi, F. Narumi, N. Iki, T. Hattori and S. Miyano, *Chem. Rev.*, 2006, **106**, 5291-5316.
29 M. Liu, W. P. Liao, C. H. Hu, S. C. Du and H. J. Zhang, *Angew. Chem. Int. Ed.*, 2012, **51**, 1585-1588.
30 K. Xiong, F. Jiang, Y. Gai, D. Yuan, L. Chen, M. Wu, K. Su and M. Hong, *Chem. Sci.* , 2012, **3**, 2321-2325.
31 W. J. Bowyer, W. Y. Xu and J. N. Demas, *Anal. Chem.*, 2009, **81**, 378-384.
32 D. A. Dougherty and D. A. Stauffer, *Science*, 1990, **250**, 1558-1560.
33 D. A. Dougherty, *Science*, 1996, **271**, 163-168.
34 J. C. Ma and D. A. Dougherty, *Chem. Rev.*, 1997, **97**, 1303-1324.
35 L. Li, S. Zhang, L. Xu, Z.-N. Chen and J. Luo, *J. Mater. Chem. C*, 2014, **2**, 1698-1703.
36 H. Pasalic, A. J. A. Aquino, D. Tunega, G. Haberhauer, M. H. Gerzabek and H. Lischka, *J. Mol. Model*, 2017, **23**, 131.
37 G. M. Sheldrick, *SHELX97 - Programs for Crystal Structure Analysis (Release 97-2)*, Institüt für Anorganische Chemie der Universität, Tammanstrasse 4, D-3400 Göttingen, Germany, 1998.
38 A. L. Spek, *J. Appl. Cryst.*, 2003, **36**, 7-13.
39 A. L. Spek, *Acta Cryst.*, 2009, **D65**, 148-155.
40 Y. Shao, Z. Gan, E. Epifanovsky, A. T. B. Gilbert, M. Wormit, J. Kussmann, A. W. Lange, A. Behn, J. Deng, X. Feng, D. Ghosh, M. Goldey, P. R. Horn, L. D. Jacobson, I. Kaliman, R. Z. Khaliullin, T. Kuś, A. Landau, J. Liu, E. I. Proynov, Y. M. Rhee, R. M. Richard, M. A. Rohrdanz, R. P. Steele, E. J. Sundstrom, H. L. Woodcock, P. M. Zimmerman, D. Zuev, B. Albrecht, E. Alguire, B. Austin, G. J. O. Beran, Y. A. Bernard, E. Berquist, K. Brandhorst, K. B. Bravaya, S. T. Brown, D. Casanova, C.-M. Chang, Y. Chen, S. H. Chien, K. D. Closser, D. L. Crittenden, M. Diedenhofen, R. A. DiStasio, H. Do, A. D. Dutoi, R. G. Edgar, S. Fatehi, L. Fusti-Molnar, A. Ghysels, A. Golubeva-Zadorozhnaya, J. Gomes, M. W. D. Hanson-Heine, P. H. P. Harbach, A. W. Hauser, E. G. Hohenstein, Z. C. Holden, T.-C. Jagau, H. Ji, B. Kaduk, K. Khistyaev, J. Kim, J. Kim, R. A. King, P. Klunzinger, D. Kosenkov, T. Kowalczyk, C. M. Krauter, K. U. Lao, A. D. Laurent, K. V. Lawler, S. V. Levchenko, C. Y. Lin, F. Liu, E. Livshits, R. C. Lochan, A. Luenser, P. Manohar, S. F. Manzer, S.-P. Mao, N. Mardirossian, A. V. Marenich, S. A. Maurer, N. J. Mayhall, E. Neuscamman, C. M. Oana, R. Olivares-Amaya, D. P. O'Neill, J. A. Parkhill, T. M. Perrine, R. Peverati, A. Prociuk, D. R. Rehn, E. Rosta, N. J. Russ, S. M. Sharada, S. Sharma, D. W. Small, A. Sodt, T. Stein, D. Stück, Y.-C. Su, A. J. W. Thom, T. Tsuchimochi, V. Vanovschi, L. Vogt, O. Vydrov, T. Wang, M. A. Watson, J. Wenzel, A. White, C. F. Williams, J. Yang, S. Yeganeh, S. R. Yost, Z.-Q. You, I. Y. Zhang, X. Zhang, Y. Zhao, B. R. Brooks, G. K. L. Chan, D. M. Chipman, C. J. Cramer, W. A. Goddard, M. S. Gordon, W. J. Hehre, A. Klamt, H. F. Schaefer, M. W. Schmidt, C. D. Sherrill, D. G. Truhlar, A. Warshel, X. Xu, A. Aspuru-Guzik, R. Baer, A. T. Bell, N. A. Besley, J.-D. Chai, A. Dreuw, B. D. Dunietz, T. R. Furlani, S. R. Gwaltney, C.-P. Hsu, Y. Jung, J. Kong, D. S. Lambrecht, W. Liang, C. Ochsenfeld, V. A. Rassolov, L. V. Slipchenko, J. E. Subotnik, T. Van Voorhis, J. M. Herbert, A. I. Krylov, P. M. W. Gill and M. Head-Gordon, *Mol. Phys.*, 2015, **113**, 184-215.
41 Y. Zhao and D. G. Truhlar, *Theor. Chem. Acc.*, 2008, **120**, 215-241.
42 Y. Zhao and D. G. Truhlar, *The Journal of Chemical Physics*, 2006, **125**, 194101.
43 T. H. D. Jr., *The Journal of Chemical Physics*, 1989, **90**, 1007-1023.
44 T. Kajiwara, T. Kobashi, R. Shinagawa, T. Ito, S. Takaishi, M. Yamashita and N. Iki, *Eur. J. Inorg. Chem.*, 2006, 1765-1770.
45 G. B. Ray, I. Chakraborty and S. P. Moulik, *J. Colloid. Interf. Sci.*, 2006, **294**, 248-254.
46 J. B. Birks and L. G. Christophorou, *Spectrochimica Acta*, 1963, **19**, 401-410.
47 P. Thordarson, *Chem. Soc. Rev.*, 2011, **40**, 1305-1323.
48 Z.-Q. Liu, Y. Zhao, Y. Deng, X.-D. Zhang, Y.-S. Kang, Q.-Y. Lu and W.-Y. Sun, *Sensors Actuators B: Chem.*, 2017, **250**, 179-188.
49 X.-D. Zhang, Y. Zhao, K. Chen, P. Wang, Y.-S. Kang, H. Wu and W.-Y. Sun, *Dalton Transactions*, 2018, **47**, 3958-3964.
50 F. G. Bordwell, *Acc. Chem. Res.*, 1988, **21**, 456-463.
51 I. V. Alabugin, K. M. Gilmore and P. W. Peterson, *Wiley Interdisciplinary Reviews: Computational Molecular Science*, 2011, **1**, 109-141.
52 Y. Zhao and D. G. Truhlar, *Theor. Chem. Acc.*, 2008, **120**, 215-241.
53 It should be mentioned that attempts to directly monitor the protonation process by ^{1}H NMR proved elusive, as the ^{1}H NMR spectrum of **1-Zn** featured poorly separated peaks (data not shown), likely due to aggregation of the neutral MOSC molecules in solution, an observation we previously addressed (ref. 23).

54 J. M. Headrick, E. G. Diken, R. S. Walters, N. I. Hammer, R. A. Christie, J. Cui, E. M. Myshakin, M. A. Duncan, M. A. Johnson and K. D. Jordan, *Science*, 2005, **308**, 1765-1769.
55 G. M. Loudon and J. Parise, *Organic Chemistry*, Roberts and Company Publishers, Greenwood Village, Colorado, Sixth edition. edn., 2016.

Table of Contents

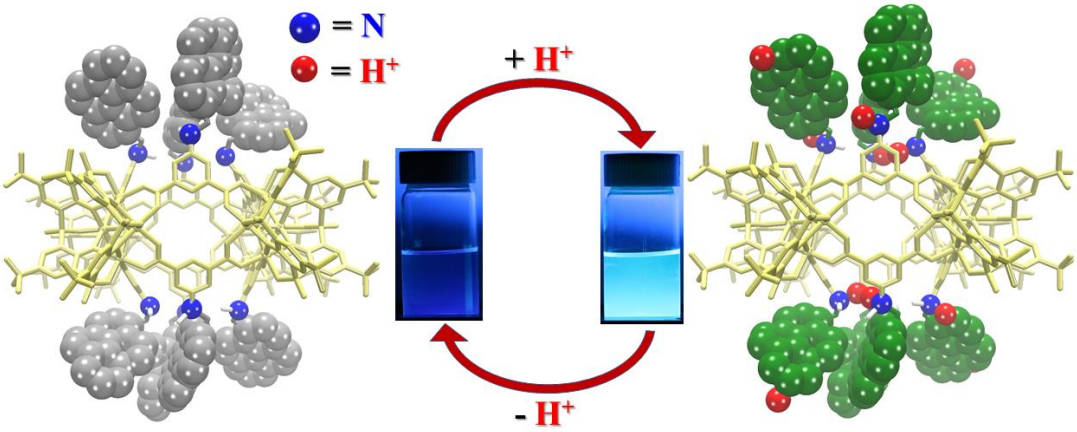

Functional supercontainers exhibit intriguing H^+-dependent fluorescent switching behavior, opening exiting new opportunities for proton modulation in both chemistry and biology.